ISTITUTO NAZIONALE DI FISICA NUCLEARE
Laboratori Nazionali di Frascati

To be submitted to
Nuclear Phys. and Meth.

LNF-80/62 (P)
9 Dicembre 1980

R. Barbini, A Cattoni, B. Dulach, C. Sanelli, M. Serio and G. Vignola:
THE LELA UNDULATOR

Servizio Documentazione
dei Laboratori Nazionali di Frascati

INFN - Laboratori Nazionali di Frascati
Servizio Documentazione

LNF-80/62(P)
9 Dicembre 1980

THE LELA UNDULATOR

R. Barbini*, A. Cattoni, B. Dulach, C. Sanelli, M. Serio and G. Vignola*
INFN - Laboratori Nazionali di Frascati, Frascati, Italy.

ABSTRACT

In this paper we present some design considerations for the LELA (Laser a Elettroni Liberi su Adone) undulator magnet (λ_q = 11.6 cm, K = 3.6, N = 20) now in construction.

We also report the measurements performed on a two periods full scale prototype magnet built in the LNF.

1. - INTRODUCTION

In the last few years there has been an increasing interest on the electromagnetic radiation emitted by electrons bent in oscillatory paths by alternate polarity magnets (undulators). Owing to the distribution of radiation in a line spectrum, one can devise to achieve, for given wavelengths, a brightness which is some order of magnitude larger than that produced by normal bending magnets (at the same wavelength).

Moreover, this radiation can be captured in an optical cavity so as to give rise to a laser oscillator (FEL): the successful experiment performed by Madey and coworkers[1] with the Stanford SCA at λ=3.4 μm showed this to be possible. On the other hand, due to the uniqueness of the experiment, it is highly desirable to collect more experimental information upon a number of items such as:

- measurement of spontaneous radiation;
- amplification of radiation with the aid of an external laser;
- wavelength and optical gain as functions of electron energy and undulator magnetic field;
- transient behaviour of laser radiation.

---

* On leave from CNEN Centro di Frascati.

Finally, since the optical gain showed to be proportional to the peak electron current, it appears attractive to investigate the FEL interaction with the aid of a high current machine such as a storage ring. To this aim a proposal[2] of a FEL experiment on Adone (LELA) has been made which utilizes an undulator installed on a straight section of the machine. Simplicity and flexibility have been the basic criteria in choosing the experiment's parameters.

Unnecessary technical complications are avoided by operating in the visible wavelength region and by adopting standard electromagnet technology. The electron energy should be the highest possible, in order to store the maximum peak current in the ring. The undulator period should be designed so as to accomodate the maximum number of periods in the fixed length (2.5 m) of the Adone straight section. Finally, electron energy, undulator period and magnetic field must satisfy the wavelength equation:

$$\lambda = \frac{\lambda_q}{2\gamma^2}(1 + K^2) \qquad (1)$$

where λ is the spontaneous radiation wavelength (first harmonic) observed along the undulator axis ($\equiv$ y axis), λ_q is the undulator period, $\gamma = E/mc^2$ and the parameter K is given by:

$$K = \frac{e\, B_{RMS}\, \lambda_q}{2\pi m\, c^2} \simeq 9.3\, B_{RMS}(KG)\, \lambda_q(m) \qquad (2)$$

B_{RMS} is the RMS vertical magnetic field on axis:

$$B_{RMS} = \left[\frac{1}{\lambda_q} \int_0^{\lambda_q} |B_z(y)|^2\, dy \right]^{1/2} \qquad (3)$$

According to the above considerations the basic LELA parameters have been chosen as follows: electron energy $E \geq 600$ MeV, radiation wavelenght $\lambda \simeq 5000$ Å, $K \geq 3.4$.

2. - DESIGN CRITERIA OF THE UNDULATOR

The factors that limit the achievable field level are the saturation of the iron, the maximum current density carried by the coils and the gap height. If one wants the emitted radiation to lie in the visible region, for an electron energy $E \geq 600$ MeV, then, according to eq. (1), any reduction of λ_q must be balanced by a corresponding increase of K (i.e. B). This is usually not allowed due to the following constraint.

By calling B_o the maximum vertical field at the gap center (pole simmetry axis) and B_p the corresponding field at the pole surface, the solution of the Maxwell equations yields[3]:

$$B_o/B_p = \frac{1}{\cosh(\zeta)} \cdot \frac{1 - \frac{\sinh(\zeta)}{3\sinh(3\zeta)}}{1 - \frac{\tanh(\zeta)}{3\tanh(3\zeta)}} \qquad (4)$$

where $\zeta = \pi/(\lambda_q/h)$.

For a fixed gap height h (see Fig. 1) there is a rapid drop in B_o/B_p as λ_q decreases. This of course reduces the value of the K coefficient because of two concurring effects as it is evident from eq. (2).

The problem is to find out the minimum λ_q which allows to reach a defined maximum B_o at the gap center for a given saturation in the iron and a given maximum permissible current density in the coils. To run a computer code in order to get a correct field map sounds obvious: nevertheless providing the code with a realistic set of input parameters will surely help in saving time and money. This is why we started with a

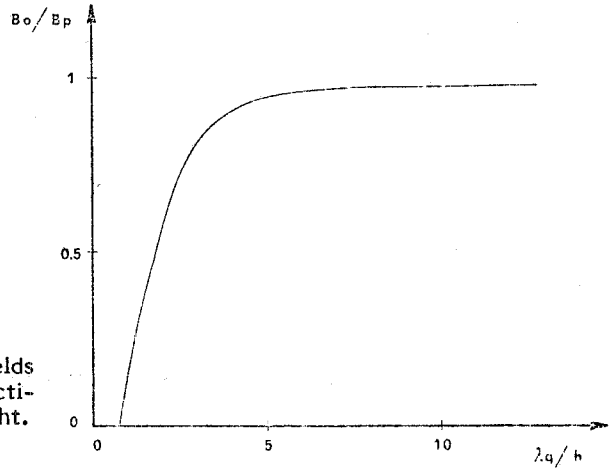

FIG. 1 - B_o and B_p are the maximum vertical fields at the gap center and on the pole surface, respectively; λ_q is the undulator period; h is the gap height.

conventional calculation of the magnetic circuit under the following assumptions:

- triangular distribution of the magnetomotive force along the pole;
- lateral permeance between adjacent poles proportional to the pole height and inversely proportional to the window width;
- saturation in the iron consistent with a B_o between 3.5 and 5.5 KG;
- current density consistent with coils made by conventional technique;
- gap height matched to the vertical aperture required in Adone.

With the geometry and symbols shown in Fig. 2 and for a cosine like magnetic field distribution in the gap

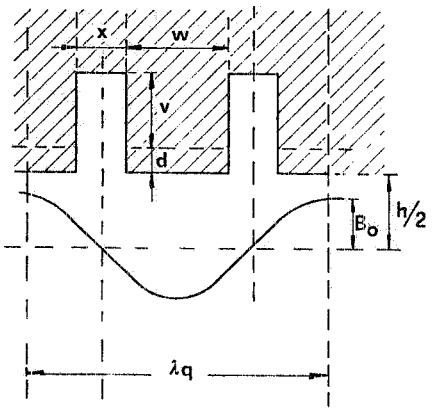

FIG. 2 - Sketch of the longitudinal magnet cut.

along the undulator axis one writes down the following system of equations:

$$k_1(w+x)+k_2\frac{v+d}{x} = w; \qquad x=k_3/v; \qquad w=\frac{\lambda_q}{2} - x \tag{5}$$

where

$$k_1=\frac{1.2\,B_o}{\sqrt{2}\,B^*}, \quad k_2=\frac{B_o h}{B^*}, \quad k_3=\frac{1.25\,B_o h}{\mu_o\, f\, S^*} \simeq 9.95 \times 10^4 \frac{B_o h}{f S^*},$$

f is the coil filling factor, d is the difference between the pole height and the coil height, B^* is the saturation

field in the iron and S^* is the max current density allowed in the coils.

The first equation accounts for the total flux carried by the pole section imposing a saturation limit equal to w B^*. The second equation comes from a balance between the amperturns applied to the circuit and the field obtained in the gap. The third equation comes from the geometry. Solving the system one gets:

$$\lambda_q = 2 \frac{(k_1 k_3 + k_3(1-k_1)) \frac{1}{v} + \frac{k_2}{k_3}(v^2 + d\,v)}{1 - k_1} \tag{6}$$

The minimum λ_q is obtained by solving the cubic equation:

$$\frac{\partial \lambda_q}{\partial v} = 2\,k_2 v^3 + k_2\,d\,v^2 - k_3^2 = 0 \tag{7}$$

This equation provides the v value to be inserted in system (5) in order to calculate x, w and the minimum λ_q. The system has been solved with the following input data:

B^* = 21 KG
S^* = 30 x 10^6 A/m^2
h = 0.04 m
f = 0.45
d = 1.2 x 10^{-2} m.

In Fig. 3 λ_q and K are plotted vs. B_o. In Fig. 4 the pole height (v+d), the half window width x/2, and the pole width w are plotted vs. B_o.

The chosen working point is B_o=4.6 KG which gives a K $\geq$ 3.4 and allows to accomodate 20 undulator periods into the Adone straight section.

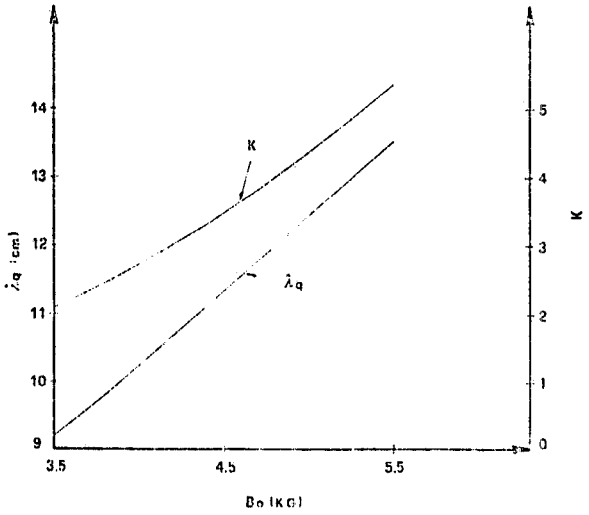

FIG. 3 - The constant K and the minimum period λ_q vs. maximum vertical field on axis B_o.

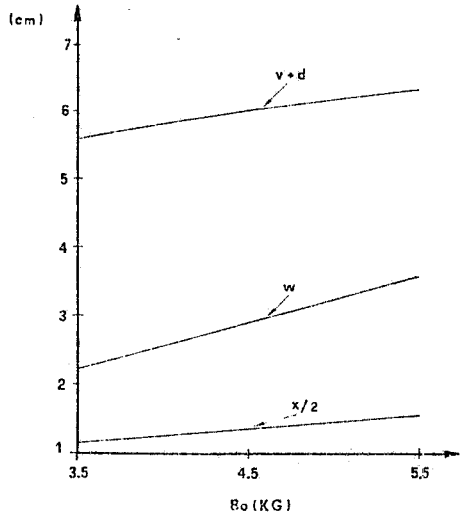

FIG. 4 - Pole height v+d, pole width w and half window width x/2 vs. maximum vertical field on axis B_o.

3. - MAGNETIC CALCULATIONS

The bidimensional magnetic field maps in the undulator have been obtained by using the CERN computer code "MAGNET"[4]. Two basic longitudinal cuts have been studied:

a) Inner Pole

For simmetry reasons it is convenient to study the field behaviour in the region shown in Fig. 5a (half inner pole), by imposing the following boundary conditions for $\vec{B}$:

- Air boundary : $B_{\perp}$ =0 along AB, $B_{//}$=0 along BC and CD;
- Iron boundary : $B_{//}$=0 along DE, $B_{\perp}$ =0 along EF and FA.

b) End Pole

In order to meet the restriction imposed by the code MAGNET[5] we studied the field map in the region shown in Fig. 6a, which depicts the full end pole plus a clamping plate plus an artificial air boundary. The boundary conditions for $\vec{B}$ are now:

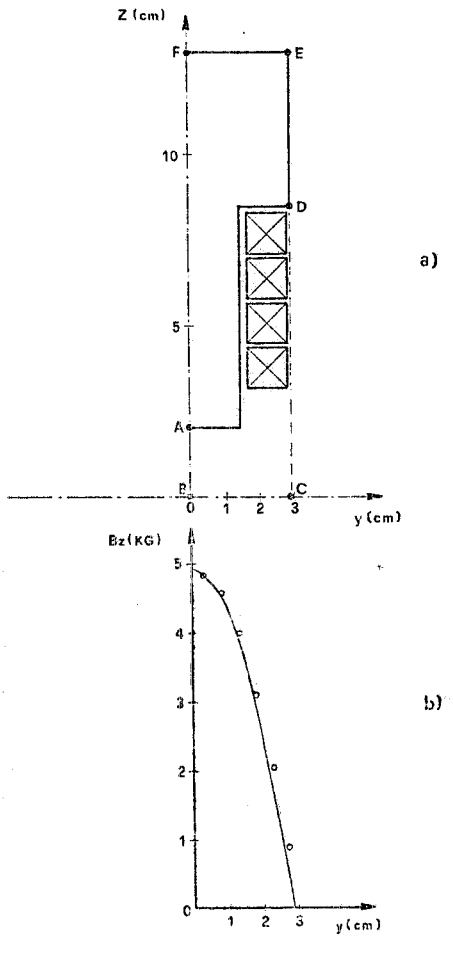

FIG. 5 - a) sketch of half an inner pole; b) vertical field on axis B_z vs. the longitudinal coordinate y. The solid curve is computed by MAGNET while the circles are measured values.

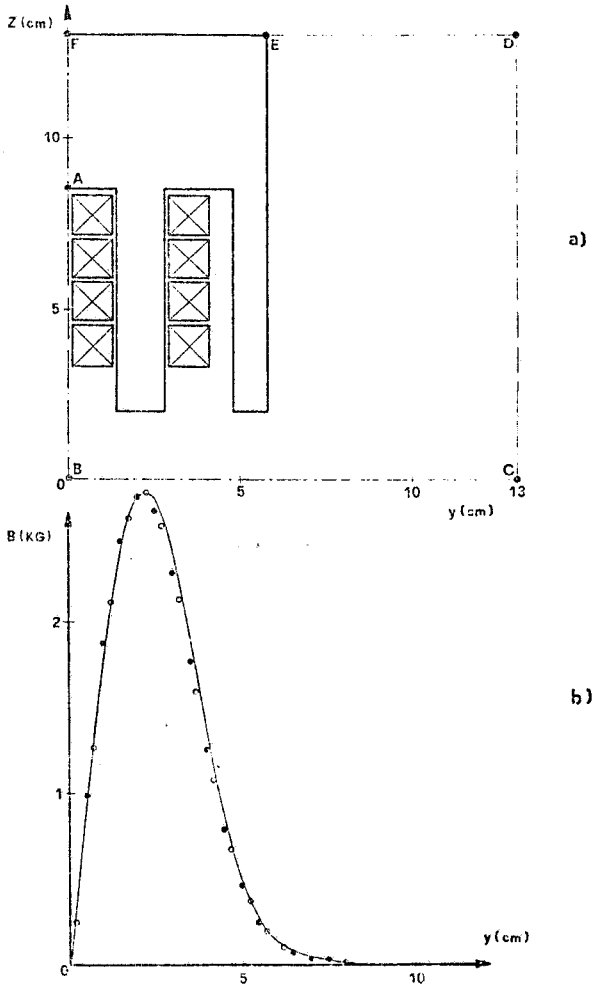

FIG. 6 - a) sketch of end pole plus clamping plate plus air boundary; b) vertical field on axis vs. the longitudinal coordinate y. The solid curve is computed by MAGNET. Circles and dots are the field values measured on the entrance and exit end poles, respectively.

- Air boundary : $B_{//}=0$ along AB and BC, $B_{\perp}=0$ along DC and DE;
- Iron boundary : $B_{\perp}=0$ along EF, $B_{//}=0$ along FA.

The artificial boundary must be chosen so as to enclose as much fringing field as possible. In practice it comes out from a compromise among various factors: actual geometrical designs, mesh size, maximum allowed number of air-iron cycles needed for reaching convergence.

The vertical field on the undulator midplane (gap center) vs. the longitudinal coordinate y as computed by MAGNET with I=3150 A and 4 turns (12600 A-turns/pole) is shown by the solid lines of Figs. 5b and 6b respectively. The points are the experimental results as measured on a full scale prototype (see par. 5). The agreement between computation and measurement is seen to be fairly good. In particular the code is able to reproduce the clamping effect of the end plate on the field, which is a valuable information insofar as the undulator is to be installed in a storage ring, requiring a vanishing field integral. Fig. 7 shows the equiflux lines plotted throughout the inner pole and the end pole plus clamping plate.

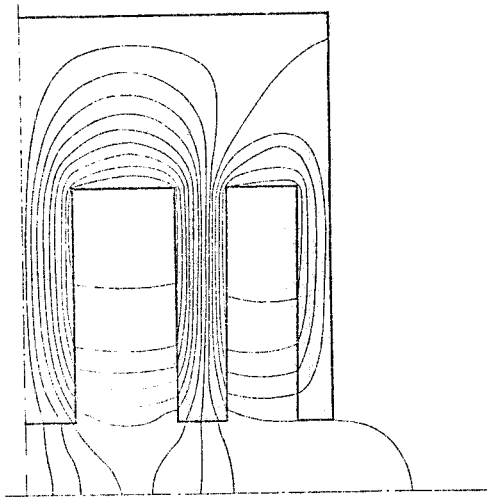

FIG. 7 - Equiflux lines plotted throughout the terminal part of the undulator (half inner pole plus end pole plus clamping plate).

4. - THE ENGINEERING OF THE UNDULATOR

Fig. 8 and Fig. 9 show the transverse and longitudinal cut of the magnet, respectively. The pole width shown in Fig. 8 is not optimized, since an exsisting stock of iron plates has been used. This large size however, ensures a large flat top in the magnetic field (along the transverse coordinate) and keeps to a minimum any perturbation due to the current returns. The magnet is built in two halves (upper and lower) for easy mounting on the Adone straight section, independently from the vacuum chamber.

A special attention has been paid in designing a mechanical structure rigid enough to keep mechanical strains and unwanted field gradients within the gap to a minimum. Taking into account both the machining tolerances and the elastic strains we expect the gap height to be $40^{+0.03}_{-0.07}$ mm. The engineering design parameters of the undulator are listed in Table I.

5. - MAGNETIC MEASUREMENTS

A double wavelength full scale prototype (3 poles + 2 half poles) of the undulator magnet has been built at LNF (see Fig. 10) in order to perform electrical and mechanical tests as well as magnetic measurements. The main goals of such measurements were to check the validity of "MAGNET" outputs with the imposed boundary conditions and to measure the RMS field and the first field integral $\int B_z\, dy$.

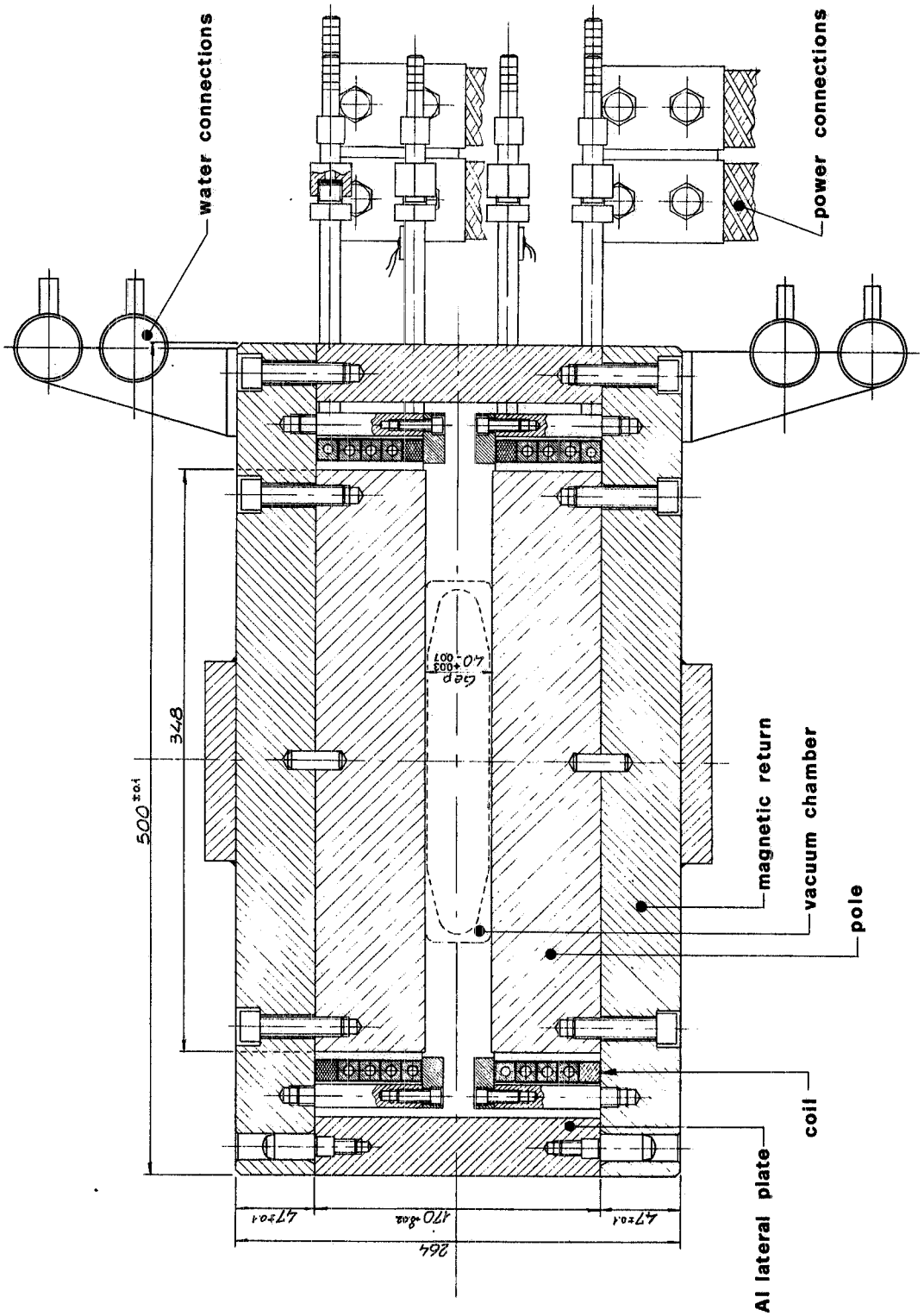

FIG. 8 - Mechanical draft of the undulator: front view.

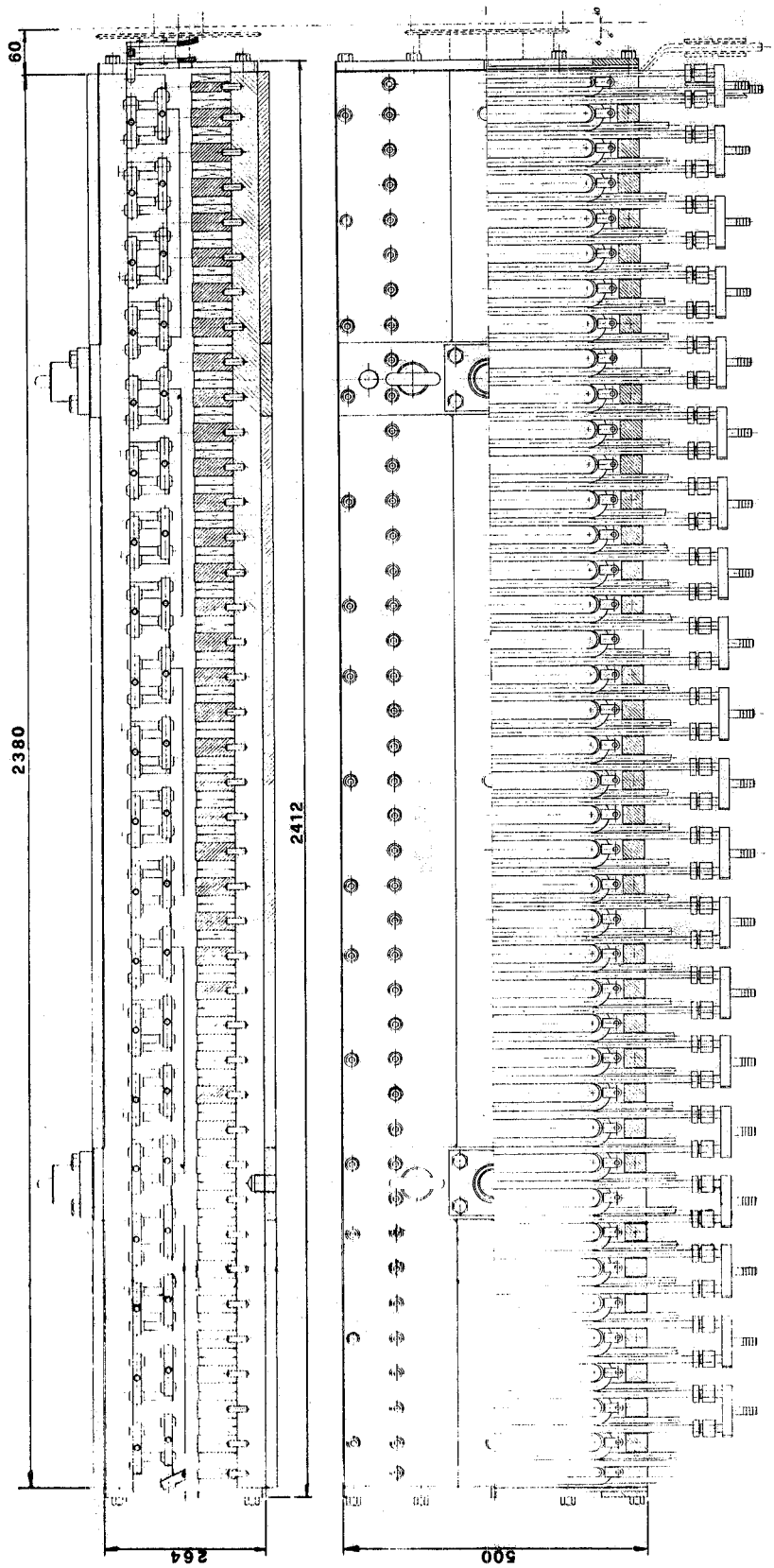

FIG. 9 - Mechanical draft of the undulator: side view.

TABLE I

UNDULATOR CHARACTERISTICS

Basic Parameters		Excitation	
Undulator period	116 mm	Excitation turns per pole	4
Number of poles	39 full poles+2 half poles	Copper conductor cross section	12 x 12 mm^2
Total length (with clamps)	2412 mm	Cooling hole diameter	7 mm
Gap height	40 mm	Copper weight	287 Kg
Pole length	29 mm	Number of water circuit	82
Pole height	65 mm	Amount of cooling water per coil	0.3 m^3/hr
Pole width	348 mm	Total amount of cooling water	25 m^3/hr
Core weight	1800 Kg	Pressure drop (all circuits in parallel)	1 Atm
Maximum field on axis	4.8 KG	Current	3150 A
		Current density	30 A/mm^2
		Total power dissipation	550 KW
		Water temperature increase	20°C

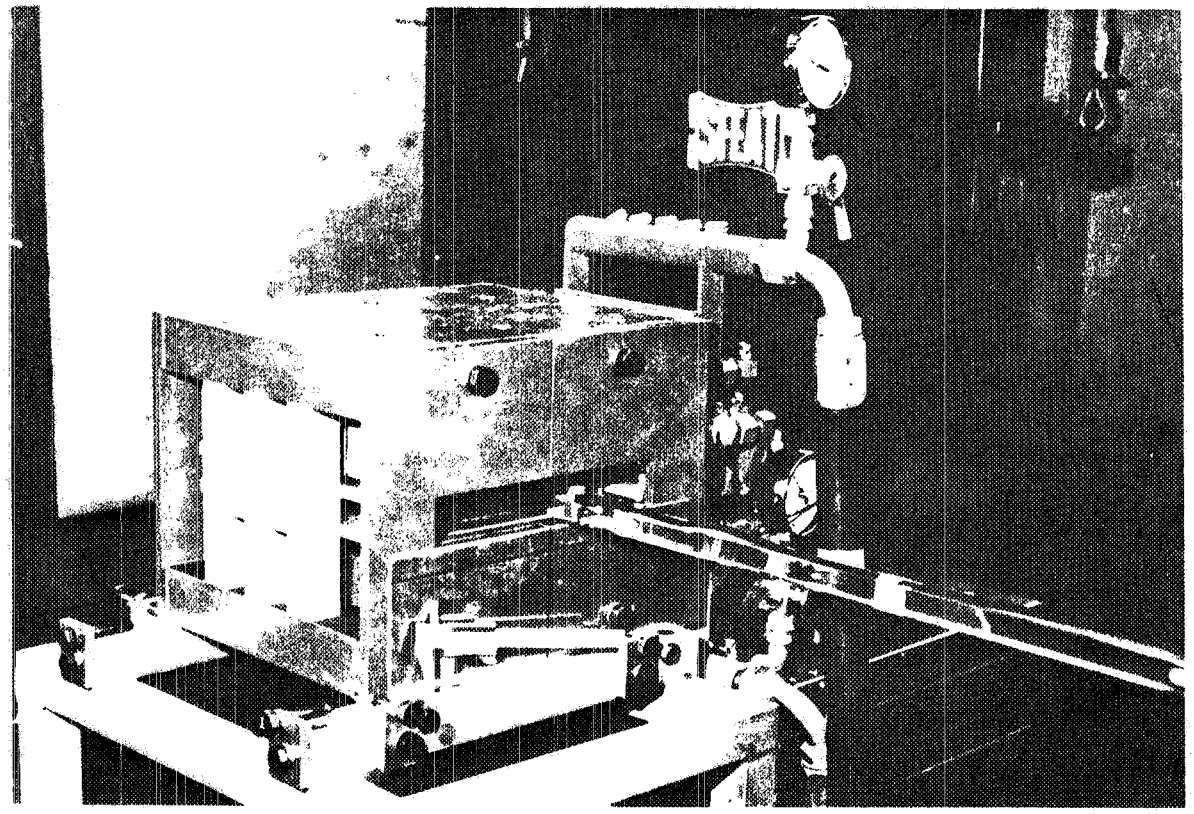

FIG. 10 - The photograph shows the undulator prototype.

The magnetic measurement layout is shown in Fig. 11.

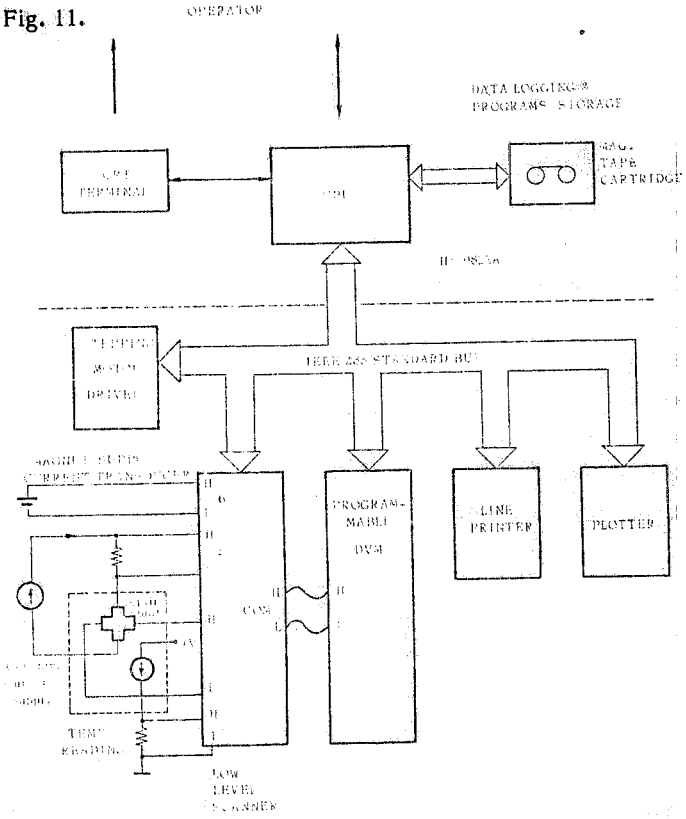

FIG. 11 - Block diagram of the magnetic measurement assembly.

Due to the highly inhomogenous nature of the field in the undulator, a 1 mm^2 Hall-Plate was chosen (SIEMENS SBV 599).

Calibration of the voltage output vs. field was performed at CERN[6] with a NMR magnetometer 9298[7], while calibration of output voltage vs. temperature was carried out at LNF, yielding a linear temperature coefficient $\simeq$ -0.1%/°C. The Hall-Plate control current is fed by a constant current generator mod. HP6181C supplying (50.000$\pm$0.002) mA. Output leads are connected through a low-level multiplexer to a high resolution DVM (mod. HP3455A) without any linearizing load resistor. The temperature is measured by means of a two terminal IC (AD590), which provides an output current proportional to the absolute temperature and insensitive to the magnetic field.

The voltage output is first corrected for temperature variations with respect to the calibration value, then converted into magnetic field value by means of a cubic spline interpolation between pairs of data points stored in a calibration array.

The instrumentation is linked through an IEEE-488 bus to a HP9825 desktop calculator which monitors the overall sequence of operations. The equipment is completed by a plotter, a line printer and a CRT display.

At the end of each scan along the longitudinal coordinate, position, Hall voltage, probe temperature and magnetic field are recorded onto a magnetic cartridge.

The control program was written in such a way as to allow for maximum interactivity during measurements, while providing some data preprocessing and plotting capabilities. More accurate numerical analysis and graphics are executed off line.

Fig. 12 shows the vertical field measured on the undulator mid-plane vs. the longitudinal coordinate y, for various currents in the coils, while the maximum field under the inner pole and the end one are plotted vs. current in Fig. 13: it is evident that saturation occurs for different current values, due to the different pole lengths. That is also clearly reflected in Fig. 14, showing the field integral vs. current: the end pole contribution

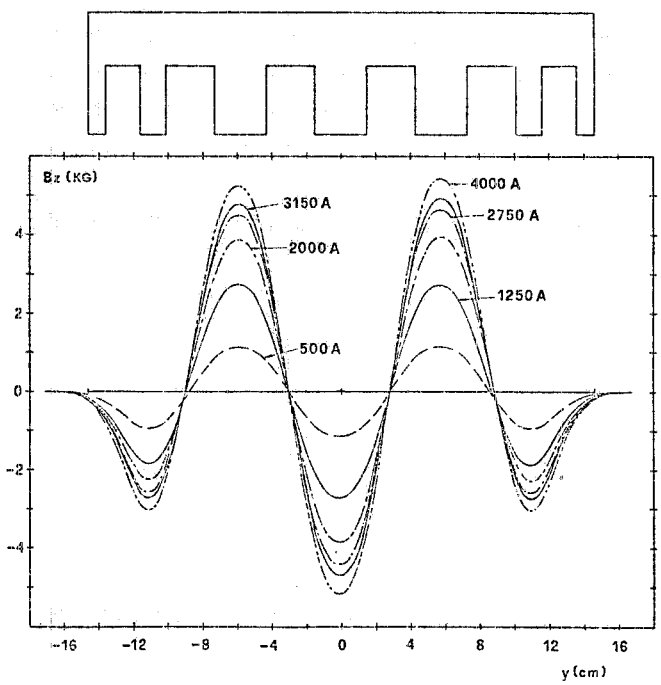

FIG. 12 - Vertical fields on axis vs. the longitudinal coordinate y. Curves are labelled by current values in the coils.

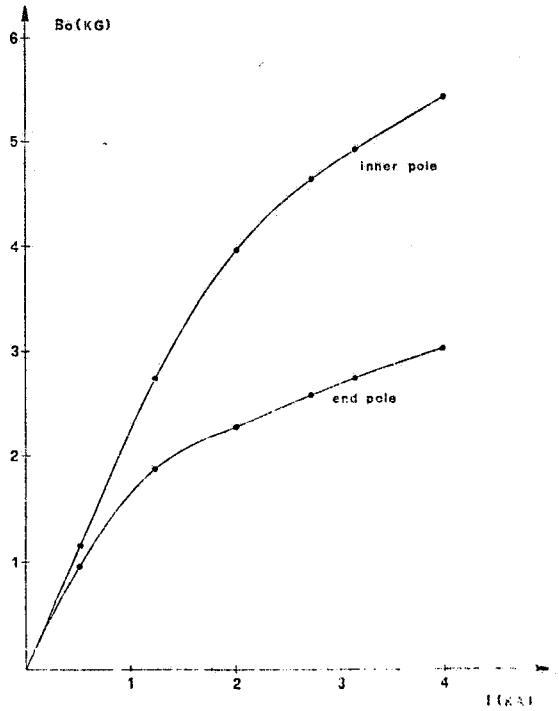

FIG. 13 - Maximum field on axis B_o vs. coil current I. The two curves are related to the inner and end pole, respectively.

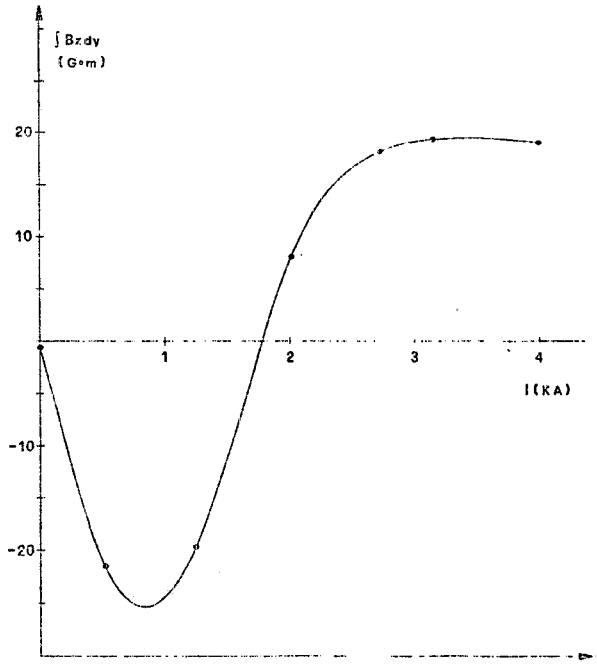

FIG. 14 - Field integral vs. the coil current I.

is prevailing up to a current region where the onset of saturation switches the integral from negative to positive. Saturation of inner poles is responsible for the constant field integral at higher currents. By varying the end pole length we are confident to rigidly lower the whole curve in order to have a nearly vanishing integral above ~ 2.5 KA. To this aim use will be made of the MAGNET code which has proven to yield an excellent matching to our experimental measurements.

Fig. 15 gives the vertical field vs. y at three different z levels for I=3150 A. By assuming the vertical field off the undulator midplane to be approximated by

$$B_z(y,z) = B_o \cos\left(\frac{2\pi}{\lambda_q} y\right) f(z) \tag{8}$$

with

$$f(z) = 1 + \alpha z^2, \tag{9}$$

we deduce

$$\alpha \approx 1.2 \times 10^{-3}\ \mathrm{mm}^{-2}. \tag{10}$$

Finally, Fig. 16 shows the K value, as defined in (2), vs. current. We notice that the design value ($K \simeq 3.4$) can actually be exceeded with no over heating of the coils.

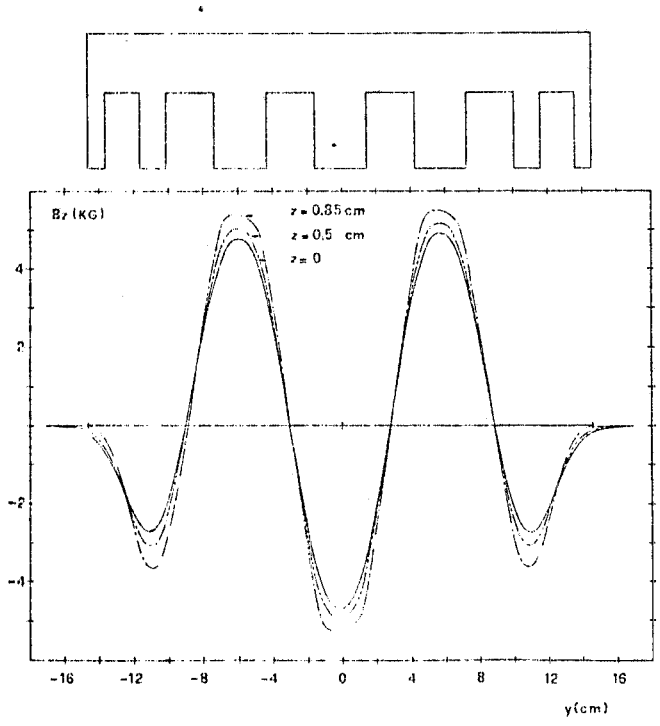

FIG. 15 - Vertical fields along the coordinate y for three values of the vertical coordinate z.

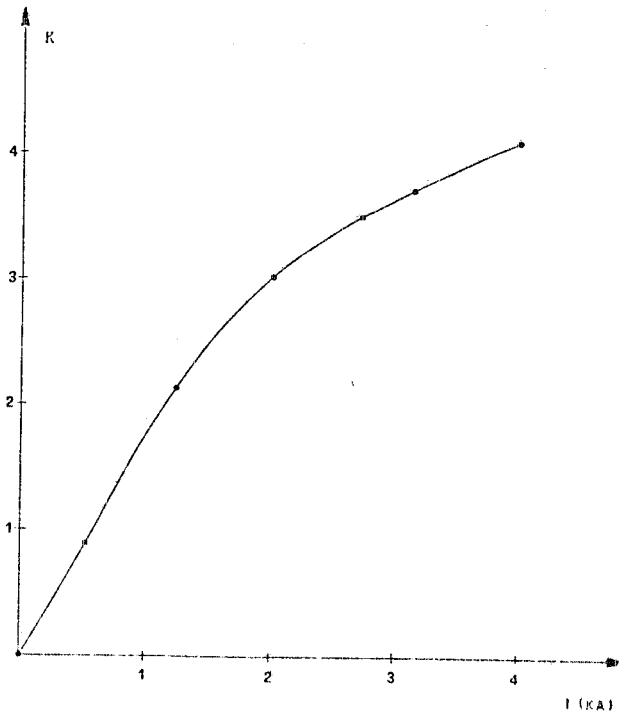

FIG. 16 - The undulator constant K vs. current in the coils.

ACKNOWLEDGEMENTS

The authors gratefully acknowledge the collaboration given by the Accelerator Division and Technical Division staffs of LNF and especially by engineers, technicians and workmen who produced the drafts, built the prototype and prepared the magnetic measurements setup.

REFERENCES

(1) D.A.G. Deacon, L.R. Elias, J.M.J. Madey, G.J. Ramian, H.A. Schwettman and T.L. Smith, Phys. Rev. Letter 38, 802 (1977).

(2) R. Barbini and G. Vignola, Frascati Report LNF-80/12 (1980).

(3) M.W. Poole and R.P. Walker, Daresbury Report DL/SCI/P215A (1980).

(4) Ch. Iselin, Program MAGNET - T600; Method described in R. Perin and S. van der Meer, Report CERN 67-7 (1967).

(5) It is not permissible to enter two or more segments of the boundary with Dirichlet conditions, separated by segments with Neumann conditions.

(6) Thanks to the courtesy of Dr. G. Frémont.

(7) K. Borer and G. Frémont, The Nuclear Magnetic Resonance Magnetometer Type 9298 Report CERN 77-19 (1977).